Flow of non-Newtonian fluids in open channels

Scott W. McCue[1] Graeme C. Hocking[2] Michael C. Dallaston[3] Luke A. Fullard[4] Peter R. Johnston[5] Agus Y. Gunawan[6] Alistair D. Fitt[7]

(Received 12 June 2015; revised 17 December 2017)

Abstract

This report details progress made in a Maths in Industry Study Group Project. The key conclusions of the study group were that correctly choosing an appropriate rheological model, and using appropriate data to compute the parameters of that model, is vital in recovering the correct fluid behaviour; and that exact mathematical solutions that exist for simplistic channel shapes can be used to approximate the flow in more complicated geometries. The problems of accurate numerical computation for highly non-Newtonian channel flow, as well as the complications that arise from turbulence, were identified as important areas of further research.

Subject class: 76A05

DOI:10.21914/anziamj.v56i0.9740, Published 2018-05-16, as part of the Proceedings of the 2014 Mathematics and Statistics in Industry Study Group. ISSN 1445-8810. (Print two pages per sheet of paper.)

Keywords: slurry, open channels, non-Newtonian flow, Bingham fluid, power-law fluid

Contents

1 Introduction

The Mathematics in Industry Study Group (MISG) project *The flow of non-Newtonian fluids in open channels* was provided by Bechtel Corporation. Bechtel Corporation is a very large construction and engineering company with significant projects in Australia. In a whole range of applications, one important issue for the Mining & Metals branch of Bechtel is the efficient handling and transportation of slurries. Typically these slurries are made up of mineral waste and clay mixed with water. Of particular interest to the present project, slurries are often transported over long distances in open channels that operate on a very slight incline, with the flow driven by gravity. A challenge for Bechtel is to be able to predict the flow rates in an open channel environment for a given slurry and channel design.

In an industrial setting, there is a preference for working with dense slurries, as the use of high volumes of water is expensive. Further, the goal of transporting slurries over long distances is normally to store them off-site after the mine has ceased operation. This storage is more easily handled if the slurry is dense, as the need for large dams is reduced.

The striking property of slurries is that, provided they are not overly dilute, they exhibit distinctly non-Newtonian behaviour; the viscosity of a slurry is not a material constant, but instead depends on the shear rate. To characterise the precise nature of this dependence, Bechtel routinely performs experiments with rheometers that measure the relationship between the shear stress applied to a specimen and the shear rate. This data is then fitted against popular non-Newtonian models, such as the Bingham plastic model, a power-law fluid, or a Herschel–Bulkley model. These models are then used to predict flow behaviour in channels and elsewhere [4].

The Bingham plastic model is characterised by a yield stress. For shear stresses below the yield stress, a Bingham plastic fluid will not flow. In the context of open channel flow, this means that there is a region of sheared flow adjacent to the channel wall and then a plug flow region that occupies

Figure 1: Schematic of an open channel flow for a slurry that obeys the Bingham plastic model. This channel has a rectangular cross-section. In the plug region the slurry moves as a rigid body. All the shearing occurs in the shear zone. The Cartesian coordinate system used in Section 3 is indicated; the flow is in the z-direction.

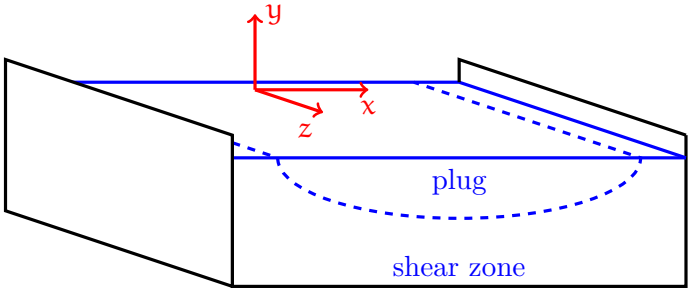

the remaining part of the cross-section of the channel (see Figure 1, for example) [6, 8]. Such plug flow regions are observed in the field, which tends to support the use of the Bingham model. Furthermore, since the Bingham model gives rise to a well-defined interface between the sheared region and the plug flow, it has the advantage of providing mathematical solutions that are straightforward to interpret. On the other hand, power-law fluids are characterised by an index. When this index is small, then a power-law fluid will flow down an open channel with an almost-plug region. In this case there will be no well-defined interface, and so notions like a plug flow are more difficult to describe objectively. The Herschel–Bulkley model is a generalisation of both the Bingham plastic model and the power-law model. Alderman & Haldenwang [1] and Burger et al. [2] discussed these non-Newtonian fluids in the context of open channel flows.

This technical report summarises progress made at the MISG meeting in February 2014 at Queensland University of Technology, and includes mathematical details. In Section 2, we present the governing equations for non-Newtonian flow of slurries. Section 3 presents some exact mathematical solutions for

flows in simple geometries. The sensitivity that these solutions have to experimentally measured parameter values is highlighted in Section 4. Section 5 reports on some numerical and approximate solutions for more complicated geometries, whereas Section 6 contains some approximate ideas to simplify the analysis on such geometries using Newtonian flow. Finally, Section 7 briefly discusses and comments on turbulent flow.

2 Non-Newtonian behaviour of slurries

2.1 Simplified constitutive laws

Typically in the engineering literature, non-Newtonian flows are described by the relationship between stress τ (Pa) and strain rate $\dot{\gamma}$ (s^{-1}) in an idealised shear flow, such as that observed in a viscometer test [9]. Constitutive laws for fluids are often described in these simple terms.

Sufficiently dense slurries appear to behave as if there is a critical yield stress, below which the slurries do not shear. In open channel flows, the non-shearing part is referred to as a plug, which is visible to the eye [10]. Perhaps the most simple constitutive description that encompasses a yield stress is that of a so-called *Bingham fluid*, also known as a yield stress fluid [9, 10, 11]. In this case the constitutive law states that

$$\begin{cases} \dot{\gamma} = 0 & \tau < \tau_{\text{yield}}, \\ \tau = \tau_{\text{yield}} + \mathsf{K}\dot{\gamma} & \tau \geqslant \tau_{\text{yield}}, \end{cases} \tag{1}$$

where τ_{yield} (Pa) is the yield stress and K is the consistency index, also known as the plastic viscosity (Pa s). This linear relationship between τ and $\dot{\gamma}$ is shown in the top-right schematic in Figure 2. In the limiting case $\tau_{\text{yield}} = 0$, such a fluid reduces to a classical Newtonian fluid and the consistency index K is equivalent to the dynamic viscosity coefficient (see the top-left schematic of Figure 2).

Figure 2: A schematic diagram indicating four different constitutive laws for slurries.

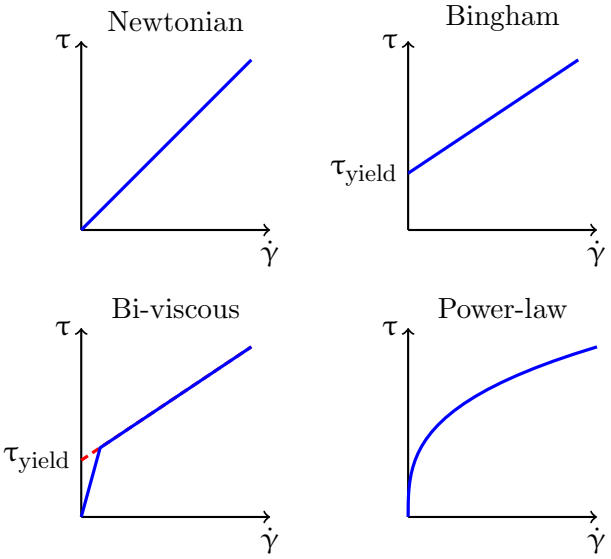

The model for Bingham fluids is not well suited for numerical analysis as the surface within the slurry that defines the transition between the plug and shear flows is not known in advance. Thus it is common for numerical solvers to approximate the Bingham model with another, such as the bi-viscous model [12] illustrated in the bottom left of Figure 2.

The Newtonian and Bingham models assume a linear relationship between stress and strain-rate. Perhaps the most simple model which is not based on such an assumption is the *power-law fluid*, for which the constitutive relationship [9] is

$$\tau = K\dot{\gamma}^{n}, \tag{2}$$

where n is a dimensionless index that characterises how non-Newtonian the slurry is. For $n > 1$ the flow is shear-thickening, a regime which does not apply for slurries. For $n < 1$ the flow is shear-thinning (see bottom right of

Figure 2 for a representative shear-thinning profile), whereas for $n = 1$ we recover Newtonian flow. The quantity K is again referred to as the consistency index, but this time the dimensions are $Pa\,s^n$.

A generalisation of both the Bingham and power-law fluids leads to the Herschel–Bulkley model [9]

$$\begin{cases} \dot{\gamma} = 0 & \tau < \tau_{yield}, \\ \tau = \tau_{yield} + K\dot{\gamma}^n & \tau \geqslant \tau_{yield}. \end{cases} \tag{3}$$

The physical parameters are defined as before. When $n = 1$ the Herschel–Bulkley model reduces to the Bingham model, whereas for $\tau_{yield} = 0$ the Herschel–Bulkley model reduces to the power-law model.

2.2 Invariant constitutive laws in three dimensions

The constitutive relationships of Section 2.1 hold only for simple flows for which the stress and strain rate depend only on one physical direction. More generally, we must work with a stress tensor $\boldsymbol{\sigma}$, written as a sum of an isotropic (hydrostatic) part, $-p\mathbf{I}$, and a deviatoric stress tensor $\boldsymbol{\tau}$. Here p is fluid pressure, and $\mathbf{I}$ is the identity tensor. In component form, this sum is

$$\sigma_{ij} = -p\delta_{ij} + \tau_{ij}\,.$$

Fully three-dimensional constitutive laws for fluids relates the deviatoric stress tensor $\boldsymbol{\tau}$ with the rate of strain tensor $\mathbf{D}$, which has components

$$D_{ij} = \frac{1}{2}\left(\frac{\partial u_i}{\partial x_j} + \frac{\partial u_j}{\partial x_i}\right),$$

where $\mathbf{u}$ is the velocity vector. For example, incompressible Newtonian fluids are defined by $\boldsymbol{\tau} = 2K\mathbf{D}$ or $\tau_{ij} = 2KD_{ij}$. For Bingham fluids the appropriate relationship is [12]

$$D_{ij} = 0, \qquad |\Pi_\tau|^{1/2} < \tau_{yield} \tag{4}$$

$$\tau_{ij} = 2\left(K + \frac{\tau_{yield}}{2\,|\Pi_\tau|^{1/2}}\right) D_{ij} \qquad |\Pi_\tau|^{1/2} \geqslant \tau_{yield}, \tag{5}$$

where here Π_τ is the second invariant of the stress tensor

$$\Pi_\tau = \tfrac{1}{2}\left[\tau_{ij}\tau_{ij} - (\tau_{kk})^2\right].$$

These relations imply that $\mathbf{D}$ and $\boldsymbol{\tau}$ are symmetric tensors. We use Einstein's summation convention which enforces summation over repeated indices. Finally, the tensor form for a power-law fluid is [14]

$$\tau_{ij} = 2K\,|4\Pi_D|^{(n-1)/2}\, D_{ij}\,,$$

where Π_D is the second invariant of the rate of strain tensor

$$\Pi_D = \tfrac{1}{2}\left[D_{ij}D_{ij} - (D_{kk})^2\right].$$

These constitutive laws reduce to the equations given in Section 2.1 for simple shearing flows.

3 Exact solutions for laminar flow

3.1 Equations of motion for simple geometries

This Section 3 is concerned with unidirectional flow down a channel which is inclined at an angle α to the horizontal. We set up a Cartesian coordinate system, as depicted in Figure 1, so that the z-axis points down the incline, with the x- and y-axes pointing horizontally and normal to the base of the channel, respectively.

In these coordinates, the equations of motions are [13]

$$\rho\left(\frac{\partial u_i}{\partial t} + u_j\frac{\partial u_i}{\partial x_j}\right) = -\frac{\partial p}{\partial x_i} + \frac{\partial \tau_{ij}}{\partial x_j} + \rho b_i\,, \tag{6}$$

where $\mathbf{x} = (x, y, z)$, ρ is density, t is time, and b_i are the body force components. Assuming the flow is driven by gravity only, $b_x = 0$, $b_y = -g\cos\alpha$ and $b_z = g\sin\alpha$.

For steady flow, only the third velocity component u_z is nonzero. If we assume the flow quantities do not depend on z, then $u_z = u_z(x, y)$, $p = p(x, y)$, and the left-hand side of (6) is zero. We are left with the single equation

$$0 = \frac{\partial \tau_{xz}}{\partial x} + \frac{\partial \tau_{yz}}{\partial y} + \rho g \sin\alpha\,. \tag{7}$$

In general, the solution of (7) depends on the constitutive equation. However, for two simple geometries we solve (7) for a general rheology.

The first of these simple geometries is known as sheet flow. In this case the channel is infinitely wide, so the shear stress τ_{xz} vanishes and the velocity depends on y only. Thus (7) reduces to

$$0 = \frac{\partial \tau_{yz}}{\partial y} + \rho g \sin\alpha\,.$$

Integrating and enforcing the condition of no shear on the free surface $y = 0$ leads to [10]

$$\tau_{yz} = -\rho g y \sin\alpha\,. \tag{8}$$

Let the sheet have a depth H; the solid boundary at $y = -H$ is the channel 'wall', giving a wall shear stress (the stress exerted on the fluid by the wall)

$$\tau_W = \rho g H \sin\alpha\,.$$

This result is true regardless of the fluid type.

The second simple geometry is flow in a channel of circular cross-section of radius R, with the slurry occupying exactly half of the cross-sectional area. In this case it is worth changing to cylindrical polar coordinates (r, θ, z). Assuming a zero stress (and therefore a zero velocity gradient) condition on the free surface, the flow field is identical to that of flow in a full circular

pipe [10]. Thus, due to rotational symmetry, the only nonzero shear stress is τ_{rz} and the axial velocity component depends only on the r direction. Under this simplification, (7) becomes

$$0 = \frac{1}{r}\frac{\partial(r\tau_{rz})}{\partial r} + \rho g \sin\alpha\,,$$

and the solution for the shear stress bounded at $r = 0$ is [10]

$$\tau_{rz} = -\tfrac{1}{2}\rho g r \sin\alpha\,. \tag{9}$$

Since the channel wall is located at $r = R$, our expression for the wall stress becomes

$$\tau_W = \tfrac{1}{2}\rho g R \sin\alpha\,. \tag{10}$$

Again, this result is not dependent on the constitutive relationship used.

3.2 Bingham fluid

We now write down some further exact results for a Bingham fluid [3]. First, for sheet flow, we denote the plug depth by H_{plug}. From (8) we immediately see that the plug has thickness

$$H_{plug} = \frac{\tau_{yield}}{\rho g \sin\alpha}\,. \tag{11}$$

Thus we need a sufficiently deep channel so that $H > H_{plug}$, or else there will be no flow. Rearranging, this condition states that we need

$$\sin\alpha > \frac{\tau_{yield}}{\rho g H}$$

to initiate flow.

We drop the subscript on the only nonzero velocity component $u_z(y)$. By substituting the Bingham law in (8) and integrating, we find

$$u(y) = \frac{\rho g \sin\alpha}{2K}(H^2 - y^2) - \frac{\tau_{yield}}{K}(y + H). \tag{12}$$

Note that we have enforced the no-slip condition $u = 0$ on $y = -H$.

Now turning to flow in a channel with semi-circular cross-section. Referring to (9) and denoting the plug depth as R_{plug}, we find

$$R_{\text{plug}} = \frac{2\tau_{\text{yield}}}{\rho g \sin\alpha}\,. \tag{13}$$

Thus for flow we need

$$\sin\alpha > \frac{2\tau_{\text{yield}}}{\rho g R}\,.$$

Now writing the velocity component by $u(r)$ we integrate (9) to find

$$u(r) = \frac{\rho g \sin\alpha}{4K}(R^2 - r^2) - \frac{\tau_{\text{yield}}}{K}(R - r). \tag{14}$$

Again, the no-slip condition is enforced on $r = R$.

3.3 Power-law fluid

Integrating (8) and (9) for a power-law fluid is reasonably straightforward. The result for sheet flow is

$$u(y) = \frac{n}{1+n}\left(\frac{\rho g \sin\alpha}{K}\right)^{1/n}\left(H^{(1+n)/n} - (-y)^{(1+n)/n}\right),$$

whereas for flow in a channel of semi-circular cross-section

$$u(r) = \frac{n}{1+n}\left(\frac{\rho g \sin\alpha}{2K}\right)^{1/n}\left(R^{(1+n)/n} - r^{(1+n)/n}\right). \tag{15}$$

For a more general cross-section, we write $u = u(x, y)$. In this case we substitute the power-law into (7) to give the nonlinear elliptic partial differential equation

$$\nabla \cdot \left(|\nabla u|^{n-1}\,\nabla u\right) = -\frac{\rho g \sin\alpha}{K} \tag{16}$$

in the relevant domain with $u = 0$ on the solid boundaries and $\partial u/\partial y = 0$ on the free surface (which we fix to be at $y = 0$). The left-hand side of (16) is known as the p-Laplacian (where, here, $p = n + 1$).

3.4 Newtonian fluid

Results for a Newtonian fluid are obtained by setting $\tau_{\text{yield}} = 0$ in the Bingham results in Section 3.2 or $n = 1$ in the power-law results in Section 3.3 to give

$$u(y) = \frac{\rho g \sin\alpha}{2K}(H^2 - y^2)$$

for sheet flow and

$$u(r) = \frac{\rho g \sin\alpha}{4K}(R^2 - r^2)$$

for semi-circular open channel flow. In the more general case, we must solve the linear partial differential equation

$$\nabla^2 u = -\frac{\rho g \sin\alpha}{K} \tag{17}$$

in the cross-sectional area with $u = 0$ on the solid boundary of the cross-section and $\partial u/\partial y = 0$ on the free surface $y = 0$.

To take one example of more complicated geometry, consider flow down a channel of rectangular cross-section with width $2L$ and depth H. In this case, the exact solution to (17) is [5]

$$u = \frac{\rho g \sin\alpha}{K}\left\{\frac{1}{2}(H^2 - y^2) + \sum_{m=0}^{\infty} \frac{16H^2(-1)^{m+1}\cos\left[\frac{1}{2}(2m+1)\pi(y/H)\right]\cosh\left[\frac{1}{2}(2m+1)\pi(x/H)\right]}{\pi^3(2m+1)^3\cosh\left[\frac{1}{2}(2m+1)\pi(L/H)\right]}\right\}, \tag{18}$$

which holds in the domain $-L \leqslant x \leqslant L$, $-H \leqslant y \leqslant 0$.

Figure 3: Shear stress (τ) versus shear rate ($\dot{\gamma}$) for a bauxite residue slurry. Data shown for three concentrations: 20% (top), 30% (middle) and 40% (bottom). Experiments performed with viscometer.

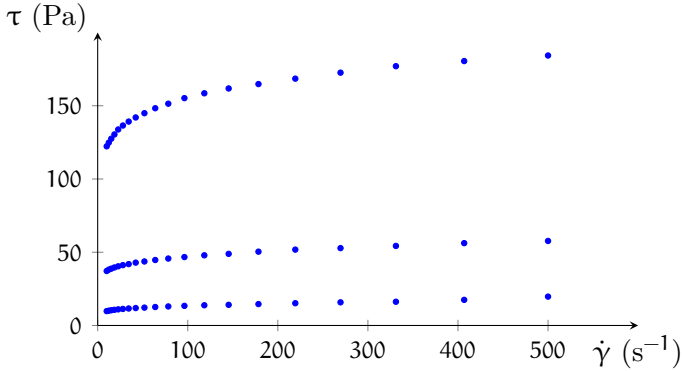

4 Behaviour of exact solutions using experimental data

4.1 Rheometer data for real slurry

During the MISG meeting, the project team was given, for a particular slurry, some data in the form of shear stress versus strain rate measurements over a range of mixture concentrations measured by mass. The slurry was made up of bauxite residue mixed with water. This data is presented in Figure 3 for three concentrations (the other concentrations showed very similar trends). We found that each set of data fitted a simple power-law extremely well, with smaller values of the index for larger concentrations. For the data shown in Figure 3, the indices were found to be $n = 0.45$ (20% kg / kg concentration), 0.16 (30% kg / kg concentration) and 0.11 (40% kg / kg concentration).

On one hand, the close fit to a power-law is a little surprising, as the Bingham model is the most popular in industry. Indeed, the Industry Representative

indicated that this slurry had been characterised as a Bingham fluid by fitting a straight line through the data and measuring the slope and intercept in the usual way. On the other hand, it is common for slurries to clearly show this type of power-law behaviour. The tendency to use a Bingham model comes from the obvious interpretation of the quantity τ_{yield} and its effect on plug size, at least in simple geometries, as discussed in Section 3.1. Furthermore, if a practitioner is able to predict the stresses that the channel flow will be operating under, then it may be easy to simply fit a line through the data in that regime. In the next subsection we show the importance of correctly choosing this regime.

4.2 Sensitivity of solutions to data fitting

To compare the different rheological models we use the exact solutions for a semi-circular channel, for both the Bingham (14) and power-law (15) fluids. The key assumption for this geometry is that the slurry is occupying the full channel, so the flow field depends on the radial distance only. For the Bingham case, the exact solution provides a simple formula for the radius of the plug region (13), which predicts that the plug radius is proportional to the yield stress but independent of the radius of the semi-circular channel. For the power-law case, the exact solution (15) provides a velocity profile that exhibits near plug flow, especially for small values of the index.

We now use these results to demonstrate how fitting data to the Bingham model requires some care. We focus on the set of data in Figure 3 corresponding to 40% concentration of bauxite residue. We re-plot this data in Figure 4, including a power law that best fits the data according to a straightforward least-squares algorithm in Microsoft Excel. Secondly, we include a fit to the Bingham model provided by the Industry Representative. With these physical parameter values, we compute the exact solutions using (14) and (15), as shown in Figure 5. The two solutions compare poorly, with the Bingham fluid model drastically underestimating the plug speed and overestimating

the plug radius, compared with the power law model.

A closer inspection of the fit in Figure 5 sheds light on this poor comparison. By noting the wall stress (10) computed with these physical parameter values is $\tau_W = \rho g R \sin \alpha/2 \approx 50\,\text{Pa}$, we observe that the straight line ((b) in Figure 4) appears to be taken to fit data points above $\tau = \tau_W$. An alternative approach is to ignore the data above τ_W and draw a line that takes in the more relevant data for the example. This line, denoted (c) on Figure 4, gives a lower yield stress τ_{yield} and a higher consistency index K, than the previous straight line fit. With these new values, we recompute the exact solution (14) for the Bingham fluid. This exact solution is depicted as (c) in Figure 5, and does closely follow the power-law solution. The conclusion is that, while this particular slurry was clearly a power-law fluid, if a Bingham model is to be used, data corresponding to the appropriate stress region (that is, those that are likely to occur in the flow itself as dependent on the driving slope) must be weighted most heavily when fitting a straight line.

5 Laminar flow in other geometries

5.1 Numerical solutions of Bingham fluids

The exact solutions mentioned in Section 3.1 apply for the special cases of an infinitely wide open channel or a full, open channel of semi-circular cross-section. For other cross-sectional shapes, we must resort to numerical solutions of the governing equations. It turns out that this computational task is more difficult than what one may first guess, for both Bingham and power-law models.

For the Bingham model, the mathematical formulation for the problem of steady flow down a open channel is not well defined. The main problem is that the Bingham model does not provide information about the stress field within the plug region. In order to make computational progress, the

Figure 4: Experimental data for shear stress τ (Pa) vs shear rate $\dot{\gamma}$ (s^{-1}) for a bauxite residue slurry, 40% concentration by mass. The data is approximated by (a) a power law model with $n = 0.11$ and $K = 28.6\,\text{Pa}\,s^n$; (b) a Bingham approximation with $\tau_{yield} = 45.5\,\text{Pa}$ and $K = .027\,\text{Pa}\,s$; (c) A Bingham approximation that ignores data for $\tau > 50\,\text{Pa}$, giving $\tau_{yield} = 40.7\,\text{Pa}$ and $K = 0.055\,\text{Pa}\,s$. The second Bingham model (c) more accurately fits the data at low stress rates, which are more likely to be seen in practice.

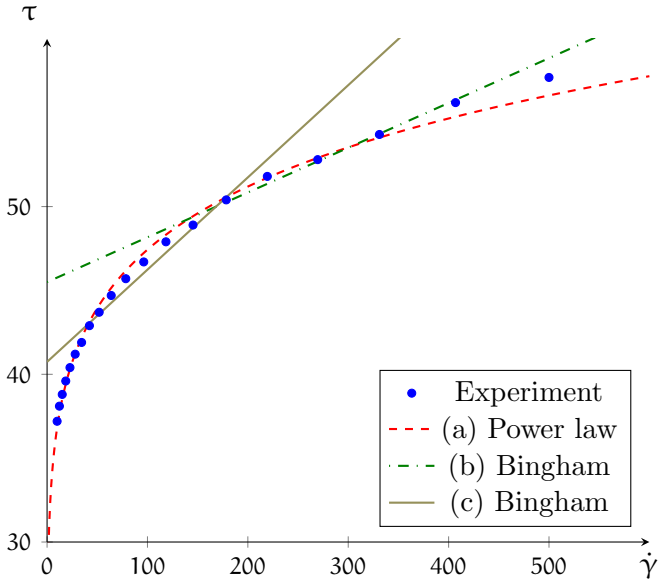

Bingham model needs adjusting so that stresses are related to shear rates throughout the flow. One common approach is to use the so-called bi-viscous model, which follows the Bingham model except for small shear rates, at which point it changes to Newtonian (Figure 2). The actual value of the shear rate at which the transition is assumed to occur is arbitrary, and not based on the properties of the actual slurry.

The project team produced numerical solutions for a slurry flowing steadily down an open channel using the finite element software package ANSYS. For

Figure 5: Exact solutions for the velocity for a semi-circular open channel with $R = 0.41\,\mathrm{m}$, $\rho = 1400\,\mathrm{kg\,m^{-3}}$, $\alpha = 1°$, $g = 9.8\,\mathrm{m\,s^{-2}}$, for power law and Bingham fluids with parameters calculated from fitting to data in Figure 4. The Bingham fluid (c) with parameters estimated from data points taken at lower shear rates is a much closer match to the power law fluid (a) than the Bingham fluid (b) with parameters estimated from data over the entire range of shear rates.

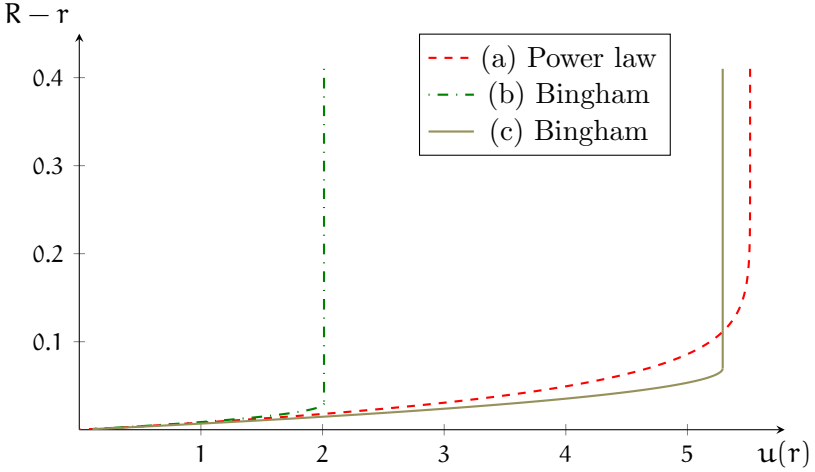

example, for a particular choice of parameter values, solutions were computed for a semi-circular channel, a rectangular channel with 2×1 aspect ratio, and a channel with large aspect ratio. These are shown in Figure 6 and Figure 7.

First, the solution in a semi-circular channel was used to compare the numerical method with the exact solution (14). The numerical scheme actually solves a bi-viscous model, and so the numerical solution for the semi-circular channel is quantitatively slightly different from the exact solution. While the results of this comparison are not shown here, we found the numerical scheme slightly overestimates the plug radius and underestimates the plug velocity. Away from the plug the comparison is very good.

The numerical solutions for the rectangular channel in Figure 6 and Figure 7 highlight the role of the two different exact solutions (12) and (14). The solution for a 2×1 rectangular channel in Figure 6 has a near-circular plug whose radius was similar to that for the semi-circular cross-section (13). In this case, we chose the area of the 2×1 rectangle to be equal to the area of the semi-circle, and the velocity profiles are reasonably similar. As the area of a 2×1 rectangular channel increases beyond this value, we find the plug becomes even more circular in shape, and the area of the plug approaches that of the semi-circular cross-section. The solution for a very wide and thin channel in Figure 7 has an almost one-dimensional plug, whose depth was one half the radius of the circular plug, and therefore close to that predicted by the exact solution for sheet flow (11). These calculations suggest a simple model for predicting the plug size and shape for laminar flow in a rectangular cross-section. That is, provided the depth of the channel satisfies $H > 2H_{plug}$ (where H_{plug} is the thickness of a plug for sheet flow, given in (11)), and provided the channel width $2L$ is such that $L \geqslant H$, then a rough estimate for the plug size is

$$\text{Cross-sectional area of plug } = 2\pi H_{plug}^2 \left(\frac{H}{L}\right) + 2LH_{plug}\left(1 - \frac{H}{L}\right)^2. \quad (19)$$

With this plug size, other key quantities like relative flow rates and hydraulic radii can be straightforwardly calculated.

5.2 Approximation for a nearly-circular channel

Instead of using numerical solutions, an approximate analytic formula may be derived for a channel cross section close to a semi-circle. Let the channel radius be given by the formula (in polar coordinates)

$$r = R^{(0)} + \epsilon R^{(1)}(\theta)$$

where ϵ is small, an approximate solution follows by linearising the equations for stress and velocity. Denoting the leading order solution (that found in Sec-

Figure 6: (a) A comparison between the centreline velocity profiles of numerically computed solutions to Bingham fluid flow in a semi-circular and a 2×1 rectangular channel. Numerically computed velocity profiles are in (b) and (c). The parameters used are $\rho = 2100\,\mathrm{kg\,m^{-3}}$, $\alpha = 10°$, $g = 9.8\,\mathrm{m\,s^{-2}}$, $\tau_{\mathrm{yield}} = 98\,\mathrm{Pa}$ and $K = 1.92\,\mathrm{Pa\,s}$. The semi-circular channel has a radius $R = 0.1\,\mathrm{m}$, while the 2×1 rectangular channel has a width $2L = 0.1772\,\mathrm{m}$ and depth $H = 0.08862\,\mathrm{m}$ (these lengths were chosen to match the cross-sectional area of the semi-circular channel).

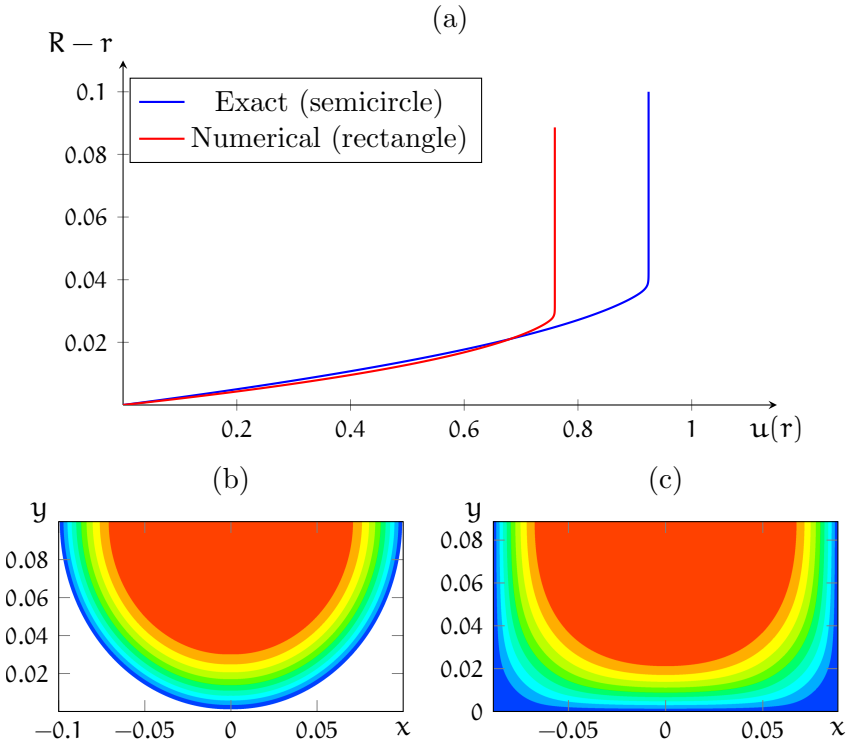

Figure 7: (a) A comparison between the centreline velocity profile of the numerically computed solution to Bingham fluid flow in a 12×1 rectangular channel with the exact solution for sheet flow (12). (b) The velocity profile from the numerical solution. The parameters used are $\rho = 2100\,\mathrm{kg\,m^{-3}}$, $\alpha = 10°$, $g = 9.8\,\mathrm{m\,s^{-2}}$, $\tau_{\mathrm{yield}} = 98\,\mathrm{Pa}$ and $K = 1.92\,\mathrm{Pa\,s}$. The 12×1 rectangular channel has a width $2L = 1.063\,\mathrm{m}$ and depth $H = 0.08862\,\mathrm{m}$.

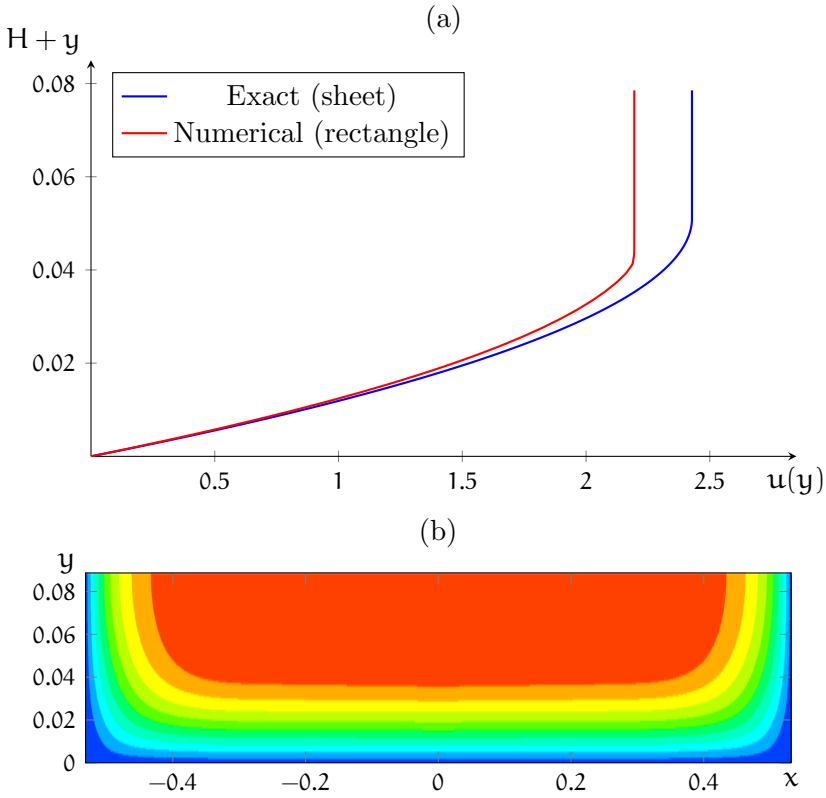

tion 3.2) with superscript (0), and all correction terms with the superscript (1), the equation for motion gives

$$\frac{\partial \tau_{rz}^{(1)}}{\partial r} + \frac{\tau_{rz}^{(1)}}{r} + \frac{1}{r}\frac{\partial \tau_{\theta z}^{(1)}}{\partial \theta} = 0\,,$$

while the correction to the stress tensor now has two components,

$$\tau_{rz}^{(1)} = K\frac{\partial u^{(1)}}{\partial r}, \qquad \tau_{\theta z}^{(1)} = \left(\frac{\tau_{yield}}{\partial_r u^{(0)}} + K\right)\frac{1}{r}\frac{\partial u^{(1)}}{\partial \theta}\,.$$

The boundary conditions on the channel wall and the plug are

$$u^{(1)} = -R^{(1)}\frac{\partial u^{(0)}}{\partial r} \quad \text{on } r = R^{(0)}, \qquad \tau_{rz}^{(1)} = -R_{plug}^{(1)}\frac{\partial \tau_{rz}^{(0)}}{\partial r} \quad \text{on } r = R_{plug}^{(0)}\,.$$

The corrections to the stress and constitutive equations must be combined into a linear second order equation for the velocity correction $u^{(1)}$, which turns out to be

$$r^2\frac{\partial^2 u^{(1)}}{\partial r^2} + r\frac{\partial u^{(1)}}{\partial r} + \left(\frac{R_{plug}^{(0)}}{r - R_{plug}^{(0)}} + 1\right)\frac{\partial^2 u^{(1)}}{\partial \theta^2} = 0\,.$$

Assume the perturbation to the boundary is a single Fourier mode: $R^{(1)} = A_k \cos k\theta$, so $u^{(1)} = f(r)\cos k\theta$ where f satisfies

$$r^2 f'' + rf' - k^2\left(\frac{R_{plug}^{(0)}}{r - R_{plug}^{(0)}} + 1\right) f = 0\,, \quad R_{plug}^{(0)} < r < R^{(0)},$$

with boundary condition

$$f(R^{(0)}) = -A_k\left(\frac{\rho g \sin\alpha R^{(0)}}{2K} - \frac{\tau_y}{K}\right).$$

This is a singular linear differential equation which has a general solution in terms of hypergeometric functions F (or polynomials of degree k). The solution that is non-singular at $r = R_{plug}^{(0)}$ is

$$f_1(r) = {}_2F_1\left([k, -k], [1], r/R_{plug}^{(0)}\right),$$

and using the boundary condition at $r = R^{(0)}$ we obtain

$$f'\left(R^{(0)}_{\text{plug}}\right) = \frac{f(R^{(0)})}{f_1(R^{(0)})} f_1'\left(R^{(0)}_{\text{plug}}\right) = -f(R^{(0)}) \frac{k^2}{R^{(0)}_{\text{plug}}} \frac{{}_2F_1\left([-k+1, k+1], [2], 1\right)}{{}_2F_1\left([-k, k], [1], R^{(0)}/R^{(0)}_{\text{plug}}\right)}$$
$$= f(R^{(0)}) \frac{k(-1)^k}{R^{(0)}_{\text{plug}} {}_2F_1\left([-k, k], [1], R^{(0)}/R^{(0)}_{\text{plug}}\right)} .$$

From the stress condition on the plug wall, the correction to the plug radius is

$$R^{(1)}_{\text{plug}} = A_k \left(\frac{R^{(0)}}{R^{(0)}_{\text{plug}}} - 1 \right) \frac{k(-1)^k}{{}_2F_1\left([-k, k], [1], R^{(0)}/R^{(0)}_{\text{plug}}\right)} \cos k\theta ,$$

or $R^{(1)}_{\text{plug}} = F\left(R^{(0)}/R^{(0)}_{\text{plug}}; k\right) R^{(1)}$, where

$$F(X; k) = (X - 1) \frac{k(-1)^k}{{}_2F_1\left([-k, k], [1], X\right)} .$$

This formula is important as it gives the effect of perturbing the wall on the shape of the plug. Note F is a rational function for integer k; the first few are

$$F(X; 1) = 1 ,$$
$$F(X; 2) = \frac{2}{3X - 1} ,$$
$$F(X; 3) = \frac{3}{10X^2 - 8X + 1} ,$$
$$F(X; 4) = \frac{4}{35X^3 - 45X^2 + 15X - 1} .$$

In all cases $F(1; k) = 1$ (if the plug is on the wall, it perturbs the same as the wall) and decreases as X increases, that is, the plug radius decreases relative to the pipe radius. The larger the value of k, the faster the decrease occurs. Thus the further the plug is from the wall, and the larger the mode number k

Figure 8: Example numerical solutions in a trapezoidal channel, for (a) a Newtonian, and (b) a power-law rheology with exponent $\mathfrak{n} = 0.14$.

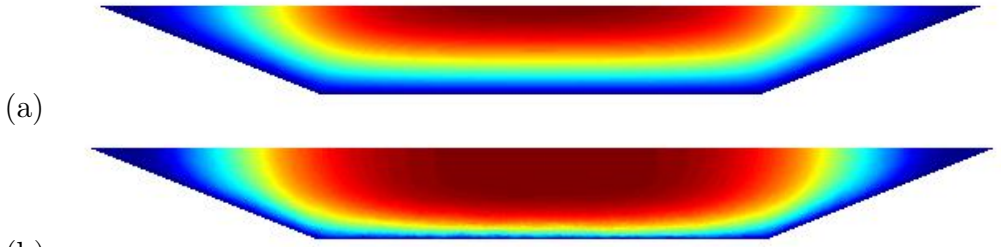

(a)

(b)

of the perturbation, the smaller the effect of the wall on the plug. This explains the numerical results in the previous section, as a $\mathsf{k} = 2$ perturbation (making a channel longer and thinner) has a much greater effect on the plug shape than a $\mathsf{k} = 4$ perturbation (making a channel more square).

5.3 Power-law fluids

Turning now to the numerical solutions with the power-law model, the project team discovered that computing solutions for fluids with a low power-law index was rather challenging. In terms of the model, the difficulties arise from the extremely high apparent viscosities at low shear rates. Regardless, solutions were computed (for moderate values of the power law index) for trapezoidal shaped channels and compared to models for Newtonian fluids (Figure 8).

6 A hybrid Bingham/Newtonian approach

An additional approach that the project team worked on was to treat the slurry as Newtonian and then stipulate a plug region that begins where the

shear stresses reach the yield stress. The advantage of this hybrid model is that the flow problems for Newtonian fluids are linear and so solved exactly by hand using traditional approaches. However, the solutions differ from the actual flow of a Bingham fluid as the stress contours do not coincide with the velocity contours, and so the flow cannot satisfy a no-slip condition on the plug wall.

We include an example using the Fourier series solution (18) for the velocity profile $u(x, y)$ in a rectangle. A typical solution, computed from this series solution, is shown in Figure 9(a). Using this solution, the stress at any location is

$$\tau = \mu \left[\left(\frac{\partial u}{\partial y} \right)^2 + \left(\frac{\partial u}{\partial z} \right)^2 \right]^{1/2} . \tag{20}$$

The stress profile corresponding to the given velocity profile is shown in Figure 9(b). The "yield" line could be any of the contours seen in this figure, that is, the line that represents those points with stresses greater than the yield stress and consequently flowing like a Newtonian fluid. The lowest stresses, as expected, are near the surface and in the centre of the channel. However, there are also regions of lower stress in the corners of the rectangular channel that reflect that the flow is slower in the corners due to the close proximity of the two boundaries, which raises the possibility that stationary plug-regions form in the corners in a true Bingham fluid flow.

Using this solution the project team estimated the flux down the channel for different values of yield stress (and the other parameters). Let the flux of the Newtonian flow over the entire domain be Q_{max}; by assuming that the flow at any point is that of the surrounding fluid where the shear is insufficient, we estimate the flux reduction as a function of yield stress for different flow parameters. Figure 10 shows plots of flux ratios for different values of $\kappa = \mathrm{Re}\,\mathrm{Fr}^{-2} \sin\alpha$, where the Reynolds number is defined as $\mathrm{Re} = V\hat{L}\rho/\mu$ and the Froude number is $\mathrm{Fr} = V/\sqrt{g\hat{H}}$. Here $\hat{L}$ is the characteristic length scale of the flow, taken here to be the depth of the rectangular channel. Each line shows the reduction in flux down the rectangular channel as the yield

Figure 9: Typical plots of (a) velocity, and (b) stress for Newtonian flow in a rectangular channel. The stress contours could form the outer zone of the "plug" flow caused by the yield stress. Highest stresses are near the walls in general, with the exception of low stress regions in the corners.

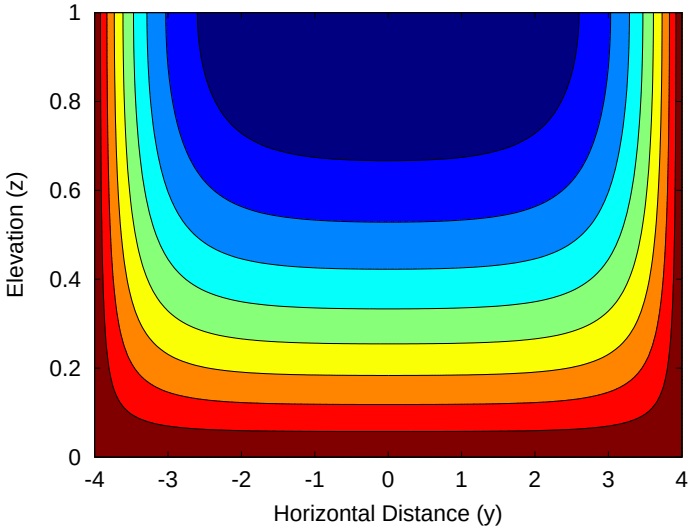

(a) Velocity

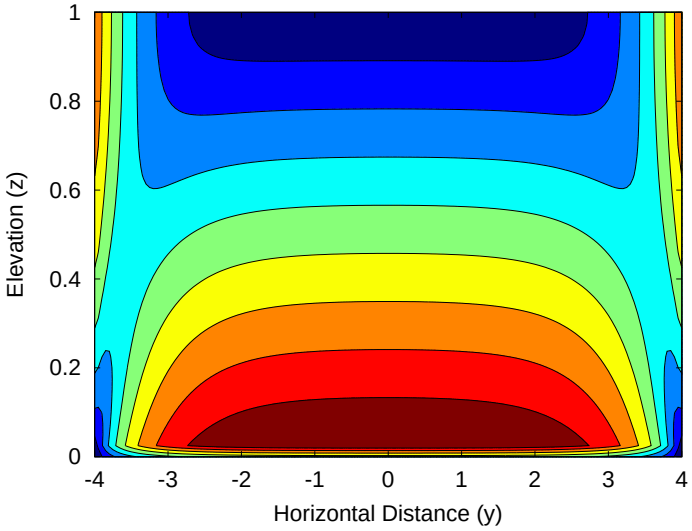

(b) Stress

Figure 10: Flux ratio for different values of yield stress at different values of flow value $\kappa = \mathrm{Re}\,\mathrm{Fr}^{-2}\sin\alpha$. Flux ratio = 1 corresponds to Newtonian flow.

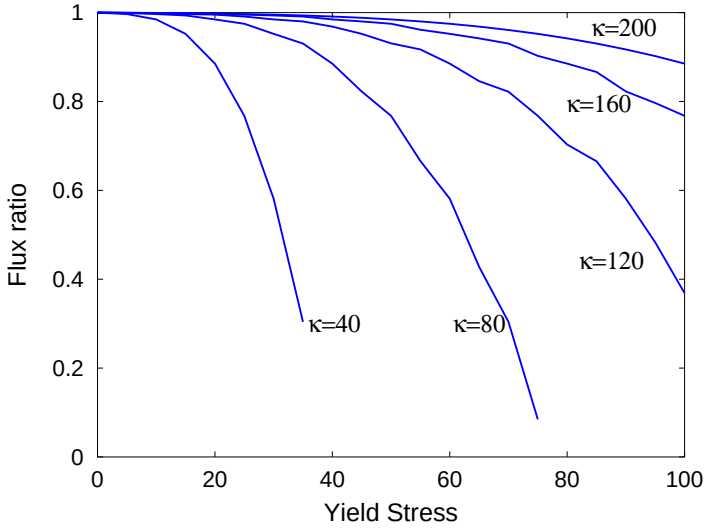

stress increases for several different values of κ. Increasing values of κ can be thought of as slightly increasing the angle of the channel. If the flow is fast enough, then the reduction in flux is quite small even for quite large values of the yield stress, whereas at small values of flow the effect is often quite dramatic. In this approximation it is difficult to compute the exact value of the "plug" velocity because the stress contours (Figure 9(b)) do not coincide with the velocity contours (Figure 9(a)), and so the local velocity profile is not accurate. However, the error is probably no greater than in the approximation of the model.

As a starting model this is probably quite reasonable and it is not difficult to compute for any cross-section shape. A more accurate representation of the "plug" component of the flow and the shear components of the flow would need to be incorporated to provide better comparison, but indications are that this approach might be used to estimate downstream fluxes for a Bingham

fluid. This work needs further attention to establish the accuracy of the approximation and to explore how the model may provide insight into the key issues with which Bechtel are concerned.

7 Discussion

The major outcomes of the study group were

- the importance of choosing an appropriate rheology, and determining the rheological parameters based on experimental data in the appropriate stress range; and
- the predictive value of the explicit solutions for semi-circular and infinite sheet geometries.

These exact solutions can closely approximate flow in other geometries, such as rectangular channels, which otherwise could only be computed numerically. We have used these approximations to derive the approximate formula (19) for the cross-sectional area of a plug region if Bingham flow is assumed. Further, it was observed during the study group that numerical computation of highly non-Newtonian flow (either due to yield stress, or small power law index) presents a serious challenge. Such numerical solutions are needed to verify the accuracy of approximate methods discussed in this report.

We close with some comments on turbulent flow. The exact and approximate solutions presented in this technical report are based on the assumption that the flow is laminar and unidirectional. That is, the assumption is that the slurry is flowing straight down the channel with no chaotic mixing behaviour. However, if the slurry is moving sufficiently quickly, then all or part of the fluid flow may be turbulent. The project team identified that the assumption of laminar flow sometimes produce speeds that are unrealistically high, because the slurries operate in a low-viscosity regime once pushed beyond the yield stress. Thus turbulent flows will frequently arise in practice.

An aspect of the problem introduced by the Industry Representative was to predict the parameter regime in which turbulence occurs, and to derive formulas for the average velocity when the flow is turbulent. For Newtonian fluids these questions are framed in terms of the dimensionless Reynolds number and friction factor. There is no universally accepted formula for these numbers for non-Newtonian fluids, although there are multiple candidates in the literature.

Although the project team did not advance to the point of deriving quantitative results during the MISG meeting itself, discussion within the team did identify avenues of further work, particularly on the Bingham model. It was reasoned that, even at sufficiently high speeds to induce turbulence, a Bingham plastic would still have a large unsheared plug, with turbulent flow restricted to a small gap between the stationary wall and the moving plug. The Reynolds number for such a flow should therefore be based on the width and characteristic viscosity inside the thin turbulent region. To construct a formula for the average velocity of the flow, the velocity profile within the thin region could be approximated using the law of the wall approximation [7] that is used for Newtonian fluid flow. Further work is needed to derive mathematical results from these preliminary observations.

Acknowledgements The problem moderators for this project were Scott McCue (Queensland University of Technology), Michael Dallaston (University of Oxford) and Graeme Hocking (Murdoch University), while the international guest was Alistair Fitt (Oxford Brookes University). The study group that contributed to this project included David Arnold, Kylie Foster, Luke Fullard, Sargon Gabriel, Bennett Gardiner, Agus Yodi Gunawan, Md Hamidul Islam, Michael Jackson, Barbara Johnston, Peter Johnston, Glen Oberman, Galyna Safonova, Stevan Stojanovic, and Jakub Tomczyk. We are grateful to Bechtel Corporation, in particular the industry representative Dr Robert Janssen, for their support of the MISG project.

References

[1] N. J. Alderman and R. Haldenwang, "A review of Newtonian and non-Newtonian flow in rectangular open channels." *Hydrotransport 17: The 17th International Conference on the Hydraulic Transport of Solids*, The Southern African Institute of Mining and Metallurgy and the BHR Group, 2007. http://hdl.handle.net/11189/5192 M120

[2] J. Burger, R. Haldenwang and N. Alderman, "Experimental database for non-Newtonian flow in four channel shapes." *Journal of Hydraulic Research*, **48** (2010): 363–370. doi:10.1080/00221686.2010.481849 M120

[3] P. Coussot, "Steady, laminar, flow of concentrated mud suspensions in open channel." *Journal of Hydraulic Research*, **32** (1994): 535–559. doi:10.1080/00221686.1994.9728354 M126

[4] D. A. Rojas and R. H. A. Janssen, "Design of open channels for non-Newtonian fluids", in *Proceedings of the 16th International Seminar on Paste and Thickened Tailings*, Eds R. J. Jewell, A. B. Fourie, J. Caldwell and J. Pimenta, Australian Centre for Geomechanics, 2013. M119

[5] S. W. McCue, J. R. King and D. S. Riley, "Extinction behaviour for two-dimensional inward-solidification problems." *Proceedings of the Royal Society of London A*, **459** (2003): 977–999. doi:10.1098/rspa.2002.1059 M128

[6] C. C. Mei and M. Yuhi, "Slow flow of a Bingham fluid in a shallow channel of finite width." *Journal of Fluid Mechanics*, **431** (2001): 135–159. doi:10.1017/S0022112000003013 M120

[7] H. Schlichting and K. Gersten, *Boundary-Layer Theory*. Springer-Verlag, Berlin Heidelberg, 2000. doi:10.1007/978-3-662-52919-5 M144

[8] K. X. Whipple, "Open-channel flow of Bingham fluids: applications in debris-flow research." *The Journal of Geology*, **105** (1997): 243–262. doi:10.1086/515916 M120

[9] R. Chhabra and J. F. Richardson, *Non-Newtonian Flow: Fundamentals and Engineering Applications*, Butterworth-Heinemann, 1999. M121, M122, M123

[10] P. Coussot, *Mudflow rheology and dynamics*, Balkema, 1997. M121, M125, M126

[11] F. Holland and R. Bragg, *Fluid Flow for Chemical and Process Engineers*, Butterworth-Heinemann, 1995. M121

[12] E. Mitsoulis, Flows of viscoplastic materials: models and computations, *Rheology reviews*, **2007** (2007), pp. 135–178. http://www.bsr.org.uk/rheology-reviews/RheologyReviews/viscoplastic-materials-Mitsoulis.pdf M122, M123

[13] D. Pritchard, B. R. Duffy, and S. K. Wilson, Shallow flows of generalised Newtonian fluids on an inclined plane, *Journal of Engineering Mathematics*, **94** (2015), pp. 115–133. doi:10.1007/s10665-014-9725-2 M124

[14] J. N. Reddy and D. K. Gartling, *The finite element method in heat transfer and fluid dynamics*, CRC press, 2010. M124

Author addresses

1. **Scott W. McCue**, Mathematical Sciences School, Queensland University of Technology, Brisbane QLD, Australia.
mailto:scott.mccue@qut.edu.au
orcid:0000-0001-5304-2384

2. **Graeme C. Hocking**, Mathematics and Statistics, Murdoch University, Perth WA, Australia.
orcid:0000-0002-5812-6015

3. **Michael C. Dallaston**, Mathematical Institute, University of Oxford, Oxford, United Kingdom (Currently: Flow Measurement and Fluid Mechanics Research Centre, Coventry University, Coventry, United Kingdom).
orcid:0000-0001-8993-6961

4. **Luke A. Fullard**, Institute of Fundamental Sciences, Massey University, Palmerston North, New Zealand.
orcid:0000-0002-9193-8664

5. **Peter R. Johnston**, Applied Mathematics, School of Natural Sciences, Griffith University, Brisbane QLD, Australia.
orcid:0000-0002-8643-3901

6. **Agus Y. Gunawan**, Industrial and Financial Mathematics Group, Institut Teknologi Bandung, Indonesia.
orcid:0000-0002-0564-1902

7. **Alistair D. Fitt**, Vice Chancellor's Office, Oxford Brookes University, Oxford, United Kingdom.
orcid:0000-0002-6109-7569